International Journal of Pharmaceutics 640 (2023) 123011

Contents lists available at ScienceDirect

International Journal of Pharmaceutics

journal homepage: www.elsevier.com/locate/ijpharm

A step forward on the *in vitro* and *in vivo* assessment of a novel nanomedicine against melanoma

Jacinta O. Pinho [a,*,1], Mariana Matias [b,*,1], Ana Godinho-Santos [a], Joana D. Amaral [a], Eduarda Mendes [a], Maria Jesus Perry [a], Ana Paula Francisco [a], Cecília M.P. Rodrigues [a], M. Manuela Gaspar [a,*]

[a] Research Institute for Medicines, iMed.ULisboa, Faculty of Pharmacy, Universidade de Lisboa, Av. Prof. Gama Pinto, 1649-003 Lisboa, Portugal
[b] CICS-UBI—Health Sciences Research Centre, University of Beira Interior, 6200-506 Covilhã, Portugal

ARTICLE INFO

Keywords:
Melanoma
Hybrid molecule
Liposomes
Cell cycle arrest
Caspase 3/7 activity
In vitro cell models
In vivo melanoma nude model

ABSTRACT

Melanoma is the most aggressive form of skin cancer, with increasing incidence and mortality rates. To overcome current treatment limitations, a hybrid molecule (HM) combining a triazene and a sulfur L-tyrosine analogue, was recently synthesized, incorporated in long blood circulating liposomes (LIP HM) and validated in an immunocompetent melanoma model. The present work constitutes a step forward in the therapeutic assessment of HM formulations. Here, human melanoma cells, A375 and MNT-1, were used and dacarbazine (DTIC), a triazene drug clinically available as first-line treatment for melanoma, constituted the positive control. In cell cycle analysis, A375 cells, after 24-h incubation with HM (60 μM) and DTIC (70 μM), resulted in a 1.2 fold increase (related to control) in the percentage of cells in G0/G1 phase. The therapeutic activity was evaluated in a human murine melanoma model (subcutaneously injected with A375 cells) to most closely resemble the human pathology. Animals treated with LIP HM exhibited the highest antimelanoma effect resulting in a 6-, 5- and 4-fold reduction on tumor volume compared to negative control, Free HM and DTIC groups, respectively. No toxic side effects were detected. Overall, these results constitute another step forward in the validation of the anti-melanoma activity of LIP HM, using a murine model that more accurately simulates the pathology that occurs in human patients.

1. Introduction

Melanoma is the most aggressive and fatal form of skin cancer, arising from the malignant conversion of melanocytes, the cells involved in melanin production (Pinho et al., 2019b). If untreated, the disease progresses and metastasizes to lymph nodes and distant organs, considerably increasing mortality (Massand and Neves, 2021). The development of this malignancy is attributed to the interaction of different factors, namely genetic (e.g. inherited mutations, polymorphisms, family history) and environmental (e.g. ultraviolet radiation, successive sunburns, use of indoor tanning, dietary factors) (Dzwierzynski, 2021; Pinho et al., 2021b). According to the International Agency for Research on Cancer, it is expected a continuous and alarming increase in the worldwide incidence (325 *vs* 425 thousand people at years 2020 *vs* 2040, respectively) and mortality (57 *vs* 85 thousand people at years 2020 *vs* 2040, respectively) of malignant melanoma (GLOBOCAN., 2022). These facts, together with the lack of effective and safe treatments, prompt the development of novel therapeutic alternatives to improve clinical outcomes.

Recently, compounds with enhanced anticancer activity have been synthesized through molecular hybridization (Alsayari et al., 2022; Aly et al., 2020; Granada et al., 2021; Sun et al., 2022). This approach combines two or more pharmacophores in one single chemical entity that acts *via* different mechanisms of action. These compounds present several advantages, such as higher affinity, selectivity and efficacy, as well as lower potential to elicit undesired side effects and ability to

* Corresponding authors.
E-mail addresses: pinho.jacinta@campus.ul.pt (J.O. Pinho), mariana.matias@fcsaude.ubi.pt (M. Matias), actgsantos@farm-id.pt (A. Godinho-Santos), jamaral@ff.ulisboa.pt (J.D. Amaral), ermendes@ff.ulisboa.pt (E. Mendes), mjprocha@ff.ulisboa.pt (M.J. Perry), afrancis@ff.ulisboa.pt (A.P. Francisco), cmprodrigues@ff.ulisboa.pt (C.M.P. Rodrigues), mgaspar@ff.ulisboa.pt, manuelagaspar@campus.ul.pt, mgaspar@ff.ulisboa.pt (M.M. Gaspar).
[1] Equal contributors.

https://doi.org/10.1016/j.ijpharm.2023.123011
Received 27 December 2022; Received in revised form 11 April 2023; Accepted 27 April 2023
Available online 3 May 2023

reduce resistances compared to monotherapy (Claudio Viegas-Junior et al., 2007; Francisco et al., 2019; Szumilak et al., 2021). Applying this promising strategy, our group has synthesized a set of hybrid molecules with antimelanoma properties. For this, 4-*S*-cysteaminylphenol (4-*S*-CAP), a L-tyrosine sulfur analogue with specific melanocytotoxicity, was combined with a triazene moiety, presenting DNA alkylating effects (Granada et al., 2021).

In particular, one of the synthesized hybrid molecules, here after designated as HM, showed the best antimelanoma properties *in vitro* (Granada et al., 2021). Indeed, a screening against several cancer cell lines revealed a higher antiproliferative activity of HM compared to temozolomide (TMZ), a triazene drug used in the clinic against melanoma brain metastasis (Pinho et al., 2023). This HM cytotoxic effect was associated to the halt of cell cycle and apoptosis of melanoma cells, as demonstrated in the murine melanoma cell line B16-F10. Further, to enhance *in vivo* therapeutic efficacy, HM was associated to long blood circulating liposomes (LIP HM). In preclinical studies using a B16-F10 syngeneic subcutaneous melanoma model, a notable reduction on tumor progression for mice treated with LIP HM was attained. Also, in a B16-F10 metastatic melanoma model, LIP HM reduced the number of lung metastases, in a higher extent as compared with Free HM (Pinho et al., 2023).

Capitalizing on the encouraging data for LIP HM (Pinho et al., 2023), in the present work we aimed to further validate this therapeutic strategy using human melanoma cell line models. HM mechanisms of actions, namely cell cycle and caspase 3/7 activity, were investigated using two human melanoma cell lines, A375 and MNT-1. Data was compared with dacarbazine (DTIC), a triazene derivative used as first-line chemotherapy for malignant melanoma (Marchesi et al., 2007; Skibba et al., 1970). For the *in vivo* therapeutic evaluation, human melanoma cells, A375, were injected subcutaneously in immunocompromised mice and four experimental groups were established: negative Control, positive control (DTIC), Free HM and LIP HM. This xenograft model provides important information regarding human disease biology and progression that, in turn, allows a more reliable prediction of patients' therapeutic response.

2. Materials and methods

2.1. Materials

Dimethyl sulfoxide (DMSO), 3-(4,5-dimethylthiazol-2-yl)-2,5-diphenyltetrazolium bromide (MTT) and dacarbazine (DTIC) were obtained from Sigma-Aldrich (St Louis, MO, USA). Cell culture media and antibiotics were purchased from Invitrogen (Life Technologies Corporation, NY, USA). Reagents for cell proliferation assays were acquired from Promega (WI, USA). The pure phospholipids egg phosphatidyl choline (PC) and distearoyl phosphatidyl ethanolamine covalently linked to polyethylene glycol 2000 (DSPE-PEG), used for the preparation of liposomal nanoformulations, were purchased from Avanti Polar Lipids (AL, USA). All the remaining chemicals used were of analytical grade. Deionized water (Milli-Q system; Millipore, Tokyo) was used in all experiments.

2.2. Animals

Male nude mice (8–10 weeks old) were purchased from Charles River (Barcelona, Spain). Animals were kept in individually ventilated cages, under strict hygiene conditions, on a 12 h light/12 h dark cycle, at 20–24 °C and 50–65% humidity. Mice had free access to sterilized diet and sterilized acidified water. All animal experiments were conducted according to the Animal Welfare Body (ORBEA) of the Faculty of Pharmacy, Universidade de Lisboa, approved by the competent national authority *Direção-Geral de Alimentação e Veterinária* (DGAV) and in accordance with the EU Directive (2010/63/UE) and Portuguese laws (DR 113/2013, 2880/ 2015, 260/2016 and 1/2019) for the use and care of animals in research.

2.3. Preparation of liposomes

Liposomes were prepared by the dehydration–rehydration method (Gaspar et al., 2015; Pinho et al., 2023), using an initial lipid concentration of 30 μmol/mL. In a round-bottomed flask, the selected phospholipids and HM at a concentration of 1 μmol/mL were dissolved in chloroform. The solvent was evaporated (Buchi R-200 rotary evaporator, Switzerland) to obtain a thin lipid film that was, subsequently, dispersed with deionized water. The so-formed suspension was frozen (-70 °C) and lyophilized (freeze–dryer, CO, USA) overnight. The lyophilized powder was rehydrated in HEPES buffer pH 7.4 (10 mM HEPES, 140 mM NaCl) in two steps, to maximize HM incorporation (Lasch et al., 2003) (Pinho et al., 2023). Using an extruder device (Lipex: Biomembranes Inc., Vancouver, Canada), the so-formed liposomal suspension was then filtered under nitrogen pressure (10–500 lb/in^2), through polycarbonate membranes of appropriate pore size until an average vesicle size of 100 nm was obtained. The separation of non-incorporated HM was performed by gel filtration (Econo-Pac® 10DG; Bio-Rad Laboratories, Hercules, CA), followed by ultracentrifugation at 250,000 *g*, for 120 min, at 15 °C in a Beckman LM-80 ultracentrifuge (Beckman Instruments, Inc, CA, USA). Finally, the pellet was suspended in HEPES buffer pH 7.4.

2.4. Characterization of liposomes

Liposomes loading HM (LIP HM) were characterized in terms of incorporation parameters, mean size and surface charge. Loading capacity was defined as the final HM to lipid ratio (HM/Lip)f and the incorporation efficiency (I.E.), in percentage, was determined according to the equation (1):

$$I.E.(\%) = \frac{\left(\frac{HM}{Lip}\right)f}{\left(\frac{HM}{Lip}\right)i} \times 100 \quad (1)$$

Phosphate content was determined using the method described by Rouser *et al.* (Rouser et al., 1970). Liposomes mean size and polydispersity index (PdI) were assessed by dynamic light scattering (Zetasizer Nano Series, Nano-S Malvern Instruments, UK) at a standard laser wavelength of 663 nm. Zeta potential of liposomal formulations was measured in a hydrodynamic sizing system (Zetasizer nano Series Nano-Z Malvern Instruments, UK).

2.5. HM quantification

The quantification of HM was performed by high performance liquid chromatography (HPLC), as described in (Pinho et al., 2023). The HPLC system was an ELITE LaChrom Hitachi (Japan), with an L-2130 pump module, a Diode-Array L-2455 detector and an autosampler L-2200 with a loop of 20 μL. The detector wavelength was set at 300 nm. The system was connected to a computer with specific software, Ez Chrom Elite, for integration and analysis of chromatograms. The analytical column was a LiChroCART® (150–4,6) Purospher® Star RP-18 (5 μm) (Merck) equipped with the respective guard-column. The mobile phase, in an isocratic solvent system, consisted of acetonitrile ACN/water (H_2O) [50:50 (*v/v*)], with a flow rate of 1 mL/min, at 25 °C. Linearity of calibration curves was ensured from 1.25 to 20 μM (R^2 = 0.9998). Samples were appropriately diluted in ACN in the range of the respective calibration curve.

2.6. Cell line culture conditions

Three human melanoma cell lines were used: commercial A375 (ATCC® CRL-1619™) and MNT-1 (ATCC® CRL-3450™), and melanoma

cells derived from biopsy samples provided by *Instituto Português de Oncologia de Lisboa Francisco Gentil* (IPO), approved by the Ethics Committee of the same institution. Cells were maintained in Dulbecco's Modified Eagle's medium (DMEM) with high-glucose (4,500 mg/L) (Sigma-Aldrich, St. Louis, MO, USA), supplemented with 10% FBS and 100 IU/mL of penicillin and 100 μg/mL streptomycin (Gibco, Thermo Fisher Scientific, Waltham, MA, USA). Cell lines were kept at 37 °C, under a 5% CO_2 atmosphere. Maintenance of cultures was performed every 2–3 days, until cells reached a confluence of about 80%.

2.7. Cell viability assay

Cell viability was evaluated in the absence (control) or presence of increasing concentrations of Free HM, LIP HM and DTIC (positive control), through the MTT assay (Pinho et al., 2021a; Santos-Rebelo et al., 2018). After reaching confluence, cells were gently detached and counted by trypan blue exclusion of dead cells, using a hemocytometer. Then, 200 μL of cell suspension, with a density of 5×10^4 cells/mL, was seeded in 96-well culture plates and left to grow for 24 h. Afterwards, complete medium was replaced, and cells were incubated with tested formulations at concentrations ranging from 10 to 75 μM, for 48 h. Cells in the presence of complete medium were used as negative control. After the incubation period, the medium was removed and cells were washed twice with 200 μL of phosphate buffer saline (PBS). Subsequently, 50 μL of the MTT solution (0.5 mg/mL), prepared in serum-free medium, were added to each well, followed by a 3 h incubation at 37 °C. The resulting formazan crystals were dissolved in DMSO and the absorbance was measured at 570 nm using a microplate reader Model 680 (Bio-Rad, CA, USA). Cell proliferation analysis was carried out in GraphPad Prism®5 (GraphPad Software, CA, USA). Values were plotted and fit to a standard inhibition log concentration–response curve.

2.8. Caspase 3/7 activity

For the evaluation of caspase-3/7 activity, A375 and MNT-1 cell lines were seeded on a 6-well plate at a density of 5×10^4 cells/mL, in 3 mL/well. After 24 h, cells were exposed to HM at 20 and 60 μM, and DTIC at 70 μM, for a period of 24 h. After incubation time, cells were detached, collected and centrifuged in PBS at 1200 *g*. Supernatants were discarded and pellets were suspended in 1 mL PBS and centrifuged at 10,000 *g*, for 1 min. The obtained pellets were air-dried and stored at −70 °C. Total protein was extracted from these pellets according to a described protocol (Pereira et al., 2016; Pinho et al., 2023, 2019a). Briefly, cell pellets were homogenized in lysis buffer containing 10 mM Tris-HCl (pH 7.6), 2.5 mM $MgCl_2$, 0.75 mM KAc, 0.5 % Nonidet P-40, 1 mM dithiothreitol (DTT) and 1 × Halt Protease and Phosphatase Inhibitor Cocktail (EDTA-free; Pierce, Thermo Fisher Scientific, Rockford, IL, USA). Samples were sonicated and centrifuged at 10,000 *g*, for 10 min at 4 °C. Supernatants were collected and stored at −80 °C. Protein quantification was performed using the Bio-Rad Protein Assay reagent, following the manufacturer's instructions. Caspase 3/7 activity was determined using the Caspase-Glo 3/7® Assay (Promega Corp., WI, USA), according to a previously established method (Pereira et al., 2016). Briefly, 15 μg of total protein extracts were incubated with the Caspase-Glo® 3/7 Reagent for 30 min, at room temperature, protected from the light. Luminescence was measured for 2 h, every 30 min, using the GloMax®-Multi Detection System (Promega Corp.).

2.9. Cell cycle distribution assay

Cell cycle distribution was determined through a standard propidium iodide (PI; Fluka, Sigma-Aldrich) staining procedure, followed by flow cytometry analysis (Pinho et al., 2023, 2021a). Briefly, a suspension of A375 or MNT-1 cells was seeded in 6-well plates at a density of 1×10^5 cells/mL, in 3 mL/well. After 24 h, cells were incubated with HM at 20 and 60 μM. Cells incubated with DTIC at 70 μM were used as positive control and cells in the presence of complete medium were used as negative control. Following 24 h of incubation, cells were detached, collected and centrifugated at 800 *g* for 5 min, at 4 °C. Cell pellets were suspended in cold PBS (500 μL), fixed with ethanol 80% at −30 °C (500 μL), under gentle agitation, and stored at 4 °C for at least 16 h. For cell cycle analysis, samples were centrifuged at 850 *g* for 5 min, at 4 °C. The obtained cell pellets were suspended in 500 μL of PBS with PI and RNase (Sigma-Aldrich) at a final concentration of 25 μg/mL and 50 μg/mL, respectively, and incubated for 30 min at 37 °C. Acquisition of 40,000 events *per* sample was performed on a full-spectrum Cytek® Aurora cytometer (Cytek Biosciences, Inc.) and data was analyzed with FCS Express™ 7 software (version 7.12.0007, De Novo software, Pasadena, CA, USA).

2.10. In vivo evaluation in a xenograft melanoma model

For xenograft melanoma tumor induction, a total of 1×10^7 A375 cells were suspended in 100 μL of PBS and injected subcutaneously in the right flank of nude (athymic) male mice (Matos et al., 2022; Pinho et al., 2019a). When tumors reached a volume of around 200 mm^3, treatment schedule was initiated. Mice were randomly divided in groups of 3–5 animals and received the formulations under study by intravenous (i.v.) route, in a total of ten administrations. Negative control group received PBS (Control), positive control group received DTIC at 10 mg/kg of body weight and the treated groups received HM in the free form (Free HM) or incorporated in long circulating liposomes (LIP HM), both at 12 mg/kg of body weight. Mice were monitored every day for pain or distress and body weight was registered. Tumor size was daily measured using a digital caliper and volumes were calculated according to the formula: $V\ (mm^3) = (L \times W^2)/2$, where L and W represent the longest and shortest axis of the tumor, respectively (Matos et al., 2022; Pinho et al., 2019a). Mice were euthanized when they met the ethical criteria for tumor size and overall health condition (loss of weight > 20%).

Three days after the final administration, mice were sacrificed, blood was collected and primary tumors were excised, weighed and a portion was stored at −80 °C for further analysis. Spleen, liver, kidneys, and lungs were excised and weighed. Tissue index was calculated according to the equation (2):

$$\text{Tissue index} = \sqrt{\frac{\text{organ weight}}{\text{animal weight}}} \times 100 \quad (2)$$

2.11. Ex vivo hepatic biochemical parameters determination

Serum was isolated from the blood and three hepatic enzymes, serum aspartate transaminase (AST), serum alanine transaminase (ALT) and serum γ-glutamyl transferase (γ-GT), were determined using a commercially available Kit (Spinreact, Spain).

2.12. Statistical analysis

Data are expressed as mean ± standard deviation (SD) for *in vitro* assays and as mean ± standard error mean (SEM) for *ex vivo* and *in vivo* assays. Statistical analysis was performed with one-way or two-way analysis of variance (ANOVA), followed by Dunnett's test, or with Mann-Whitney *U* test using GraphPad Prism version 8.0.1 for Windows (GraphPad Software, San Diego, California USA, https://www.graphpad.com). Differences between groups were considered statistically significant when $P < 0.05$. The determination of the IC_{50} was done by sigmoidal fitting analysis considering a confidence level of 95%.

3. Results

3.1. Influence of HM and DTIC on caspase 3/7 activity

The activity of effector caspases 3 and 7 was assessed as an early marker of apoptosis in human melanoma cell lines, in the absence or presence of HM (20 and 60 μM) or DTIC (70 μM). As shown in Fig. 1, no changes in caspase 3/7 activity were observed for A375 cells incubated with HM or DTIC, in comparison to control. In turn, decreased levels were attained for the MNT-1 cell line when incubated with tested compounds.

3.2. Cell cycle distribution after incubation with HM or DTIC

Cell cycle analysis revealed that incubation of A375 cells with HM at 60 μM and DTIC at 70 μM significantly increased the percentage of cells in G0/G1 phase from 57% (control) to 68 and 67%, respectively (Fig. 2). Also, this was associated with a significant decrease in the percentage of cells in S phase from 29% (control) to 20% for HM and 19% for DTIC. In the case of MNT-1 cell line, incubation with HM at 60 μM significantly increased cells in phase S (42 *vs* 29% control) while the presence of DTIC at 70 μM did not affect cell cycle (Fig. 2). In Figure S1, and for both cell lines under study, representative histograms, for all tested samples, automatically generated are depicted.

3.3. Antiproliferative properties of HM formulations and DTIC

The herein developed HM-loaded liposomes (LIP HM) displayed high incorporation parameters, with a loading capacity of 38 ± 2 nmol/μmol of lipid and an incorporation efficiency (I.E.) of 100%. A mean size of 100 nm (PdI < 0.1) and a surface charge close to neutrality (−3 ± 1 mV) were obtained (Table S1). The antiproliferative activity of Free HM, LIP HM and DTIC towards the three human cell lines under study was assessed through the MTT assay following 48 h of incubation. The obtained half-inhibitory concentration values (IC_{50}) are depicted in Table S2. For A375 and MNT-1 cells, IC_{50} values of 38.7 and > 75 μM for Free HM have been previously reported (Pinho et al., 2023). In the present work, incubation of IPO cells with Free HM resulted in an IC_{50} of 25 μM. In turn, values > 75 μM were obtained for all analysed cell lines when incubated with LIP HM or DTIC.

3.4. Therapeutic efficacy of tested formulations

During the *in vivo* experimental protocol, all mice were monitored in terms of behavior, tumor volume and body weight. As seen in Fig. 3a, animals receiving i.v. administrations of LIP HM at 12 mg/kg of body weight showed a significant impairment in tumor progression, with a final tumor volume of 265 ± 84 mm^3 compared to values of 1612 ± 550 mm^3 ($P = 0.0040$), 1309 ± 403 mm^3 ($P = 0.0152$) and 1031 ± 235 mm^3 ($P = 0.0159$) for Control, Free HM and DTIC groups, respectively. DTIC-treated animals displayed a tumor volume of 1031 ± 235 mm^3. In terms of average tumor weight, at the end of the experimental protocol (Fig. 3b), all groups were significantly different from LIP HM, that displayed the lowest value (0.4 ± 0.1 g). For Control, Free HM and DTIC groups, values of 1.2 ± 0.5 g, 1.1 ± 0.3 g and 0.9 ± 0.2 g were obtained, respectively. As shown in Fig. 3c, all animals displayed a similar body weight change over the course of the protocol, with no marked variations. Further, the assessment of caspase 3/7 activity in total protein extracts of melanoma tumors revealed a significant increase in mice treated with LIP HM (2.3 ± 0.5), as compared with Control group (1.0 ± 0.2) (Fig. 3d).

3.5. In vivo safety parameters

At the end of the experimental protocol, tissue indexes and hepatic enzymes AST, ALT and γ-GT were evaluated as safety parameters in the xenograft murine melanoma model. As depicted in Fig. 4a, no changes were observed among tested groups relating to tissue index of major organs, namely liver, spleen, kidneys and lungs. Moreover, despite differences among groups under study, the serum levels of enzymes γ-GT (Fig. 4b), as well as AST and ALT (Fig. 4c) for all animals, were within reference intervals (Charles River Laboratories, 2012; Miguel et al., 2022; Yang et al., 2020). Significant lower values of AST were obtained for animals receiving LIP HM (4.5 ± 0.8 U/L), compared to Control (9.4 ± 1.8 U/L), Free HM (10.0 ± 0.9 U/L) and DTIC (11.3 ± 1.8 U/L) groups. In terms of AST/ALT ratio (Fig. 4d), a value < 1 was observed for animals treated with LIP HM, while values of 1.8 ± 0.4, 2.0 ± 0.4 and 2.6 ± 0.6 were obtained for Control, Free HM and DTIC groups, respectively.

4. Discussion

In the drug development pipeline, cultured cell lines are important biological models for the primary *in vitro* screening of candidate anticancer molecules. This allows to determine the potency of tested compounds, as well as to unveil the mechanisms of action. Different cell lines have been used as platforms in preclinical studies aiming to provide a closer representation of clinical situations. Previously, our research group has assessed the therapeutic potential of HM formulations using the murine melanoma cell line B16-F10. In the present work, two commercial human melanoma cell lines A375 and MNT-1, with different characteristics, as well as patient-derived cells, were employed, with the

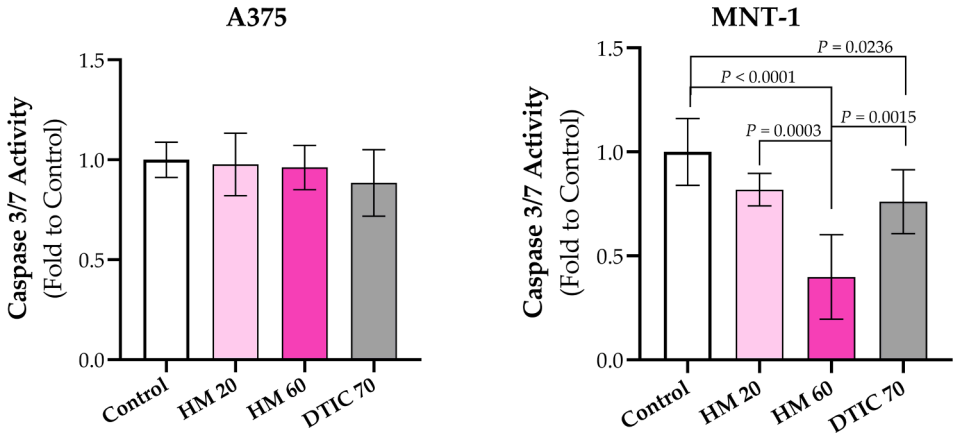

Fig. 1. Caspase 3/7 activity determined in protein extracts from human melanoma cell lines, A375 and MNT-1, after incubation with HM at 20 and 60 μM and DTIC at 70 μM, for 24 h. Statistics were performed with one-way ANOVA followed by Dunnett's *post-hoc*. Data are expressed as mean ± SD (n = 6–9).

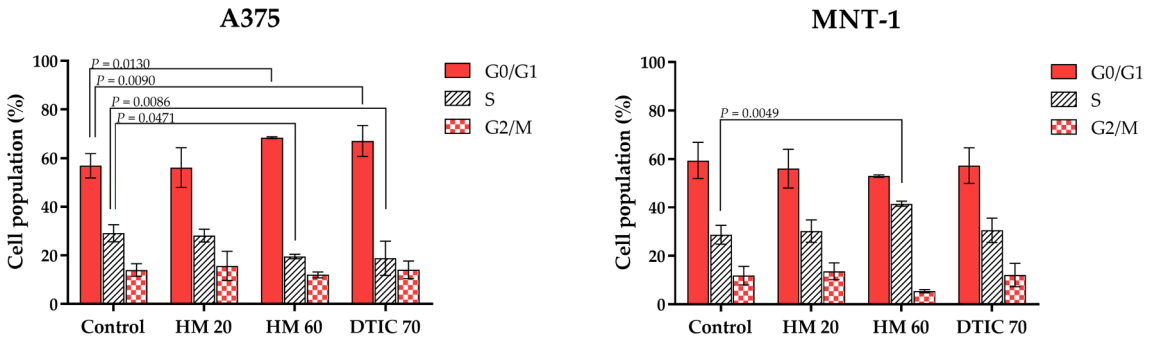

Fig. 2. Quantitative analysis of the gated A375 and MNT-1 melanoma cells in the G0/G1, S, and G2/M phases of cell cycle in the absence (Control) or presence of HM at 20 and 60 μM or DTIC at 70 μM. A total of 40,000 cells *per* sample were analyzed. Statistics were performed with two-way ANOVA followed by Dunnett's *post-hoc*. Data are expressed as mean ± SD ($n = 2$).

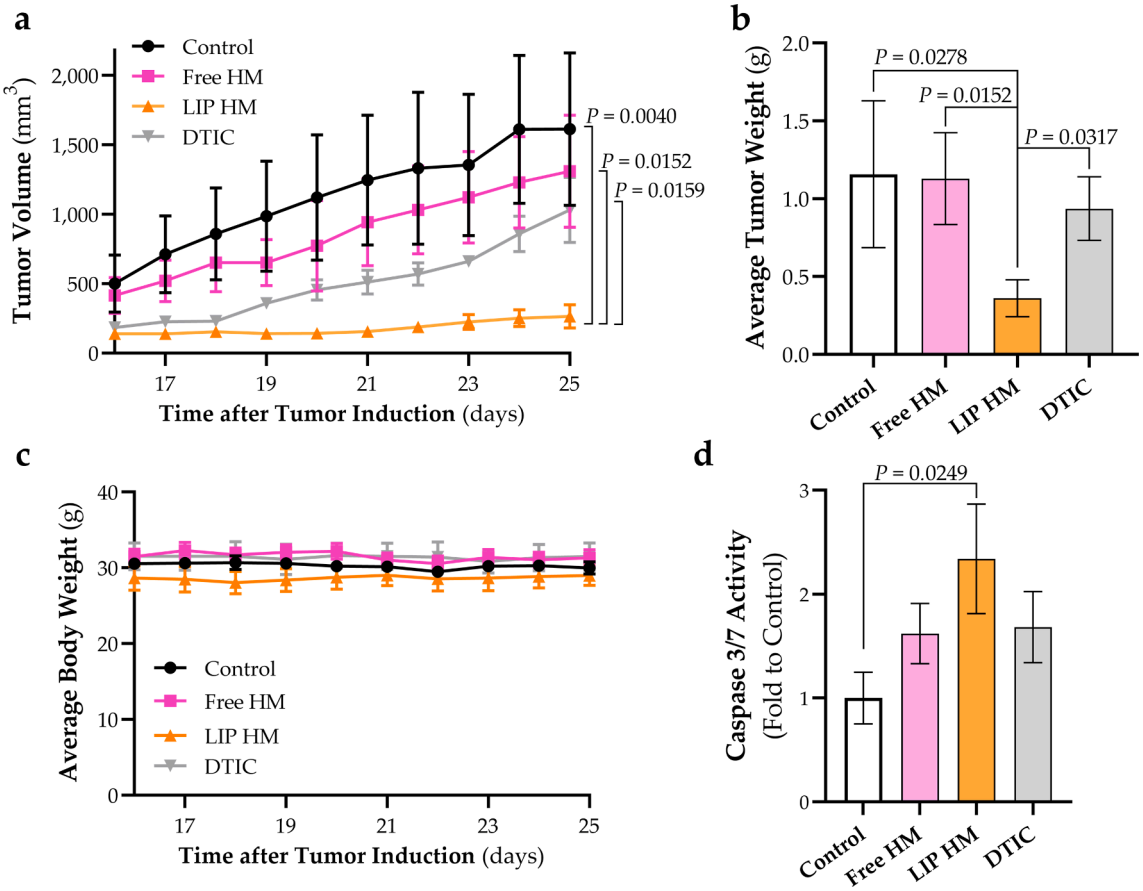

Fig. 3. A375 xenograft melanoma mouse model. After 16 days of tumor induction, treatment schedule was initiated. C57Bl/6 mice received i.v. administrations of PBS (Control), HM in free (Free HM) or liposomal (LIP HM) forms, at a dose of 12 mg/kg of body weight, and dacarbazine (DTIC) at a dose of 10 mg/kg of body weight in a total of ten consecutive administrations. **(a)** Mean tumor volume. *P* values correspond to day 25 after tumor induction. *P* values correspond to the final treatment administration. **(b)** Mean tumor weight. **(c)** Mean body weight change for all groups. **(d)** Caspase 3/7 activity determined in protein extracts from melanoma mass tumors. Statistics were performed with Mann-Whitney *U* test. Data are expressed as mean ± SEM ($n = 4$–6).

purpose of representing the human melanoma heterogeneity (Matias et al., 2021).

An important feature of melanoma is the deregulated melanogenesis, the process of melanin production mediated by the enzyme tyrosinase (Matias et al., 2021). In the melanotic cells B16-F10 and MNT-1, tyrosinase activity is higher compared to the amelanotic A375 cell line (Pinho et al., 2023). However, in the clinic it is well-established that even in amelanotic melanoma cases, tyrosinase activity is also detected, (Jimbow et al., 2013). In fact, amelanotic tumor lesions are frequently associated to a rapid growth rate and aggressive profile (Liu et al., 2006; Thomas et al., 2014). This is supported by *in vitro* migration studies that have demonstrated the significantly higher migratory ability of commercial amelanotic A375 cells, compared to the melanotic MNT-1 cells (Barrionuevo et al., 2020; Li et al., 2019; Militaru et al., 2023; Rossi et al., 2018). Literature reports also emphasize the different drug responses between amelanotic and melanotic cell lines, as well as among only melanotic cells. For instance, Rok and colleagues showed that tetracyclines displayed around 20 fold- higher EC_{50} values towards amelanotic melanoma cells (A375 and C32) compared to melanotic cells, COLO829 (Rok et al., 2022). However, A375 cells were more sensitive to

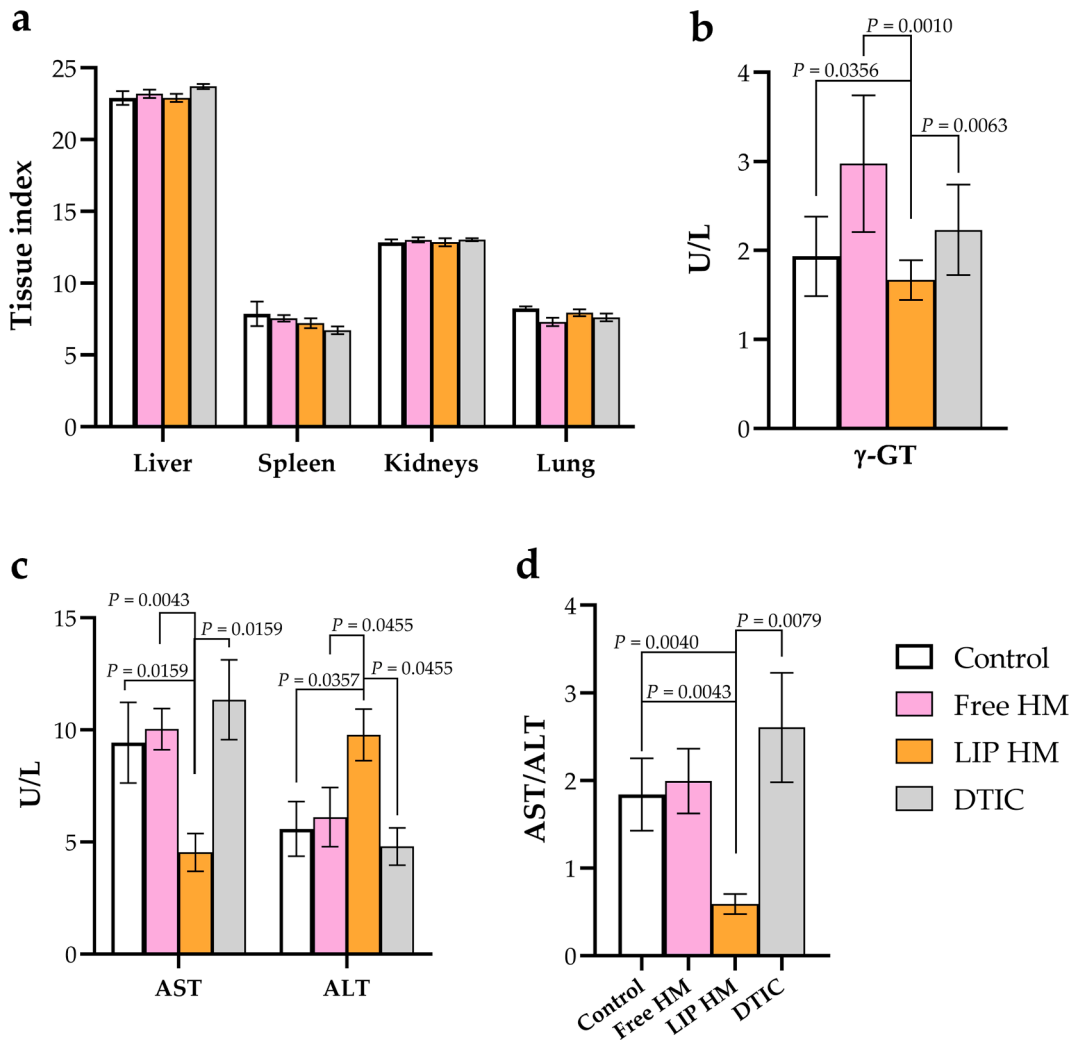

Fig. 4. Safety parameters evaluated in the xenograft melanoma mouse model, from the blood collected at the end of the experimental protocol. **(a)** Tissue index for liver, spleen, kidneys, and lung. **(b-d)** Assessment of liver function by evaluating the enzymes γ-GT, AST and ALT. Statistics were performed with Mann-Whitney *U* test. Data are presented as mean ± SEM (n = 4–6).

tetracyclines than C32 cell line (approximately a two-fold lower EC_{50} value) (Rok et al., 2022). Furthermore, Bratu and collaborators have found that non-pigmented SK-MEL-5 cells were more susceptible to betulinic acid treatment than pigmented B16-F10 melanoma cells (Bratu et al., 2022). These data indicate the protective role of melanin against external agents, also contributing to the variable *in vitro* responses observed for cell lines of different origins. Our data is in accordance with these reports, since IC_{50} values for amelanotic A375 cells were lower than those obtained for melanotic cell lines MNT-1: 38.7 and > 75 μM, respectively (Table S2).

The altered melanogenesis process leads to a mutagenic and immunosuppressive tumor microenvironment, promoting genetic instability and the emergence of more aggressive and therapy-resistant melanoma cells (Brożyna et al., 2013; Slominski et al., 2004, 2022). A genetic hallmark of human melanoma is the mutated B-raf proto-oncogene serine/threonine-protein kinase (BRAF) gene. This is a genetic alteration observed in>50% of all advanced melanoma cases, with $BRAF^{V600E}$ (valine substitution at codon 600) corresponding to 90% of all reported BRAF mutations (Ito et al., 2021; Ryabaya et al., 2019; Sun et al., 2014). Importantly, melanoma patients treated with BRAF inhibitors often develop resistance to treatment, representing a major obstacle in clinical practice (Sun et al., 2014). Comparing the genetic profile of the cell lines used in our previous and present work, only A375 and MNT-1 cells carry the $BRAF^{V600E}$ mutation (Makowiecka et al., 2016; Ryabaya et al., 2019, 2021; Sweeny et al., 2016), opposed to the murine B16-F10 cells that lack this genetic alteration (Jia et al., 2020; Melnikova et al., 2004). Interestingly, researchers have found that, among six different cell lines of advanced disease, MNT-1 cells presented the most similar gene expression profile as normal melanocytes (Hoek et al., 2004).

Overall, these different *in vitro* results, for each particular melanoma cell line, demonstrate the high heterogeneity of melanoma thus requiring the use of a high variety of cell lines when assessing the therapeutic potential of a new therapy.

The mode of action underlying the anticancer effects of HM and DTIC, considering caspase 3/7 activity and cell cycle distribution, were assessed. The rational for using DTIC as positive control was due to the fact that this triazene derivative is the only i.v. chemotherapeutic drug clinically approved for melanoma (Granada et al., 2021; Marchesi et al., 2007; Matias et al., 2021; Pinho et al., 2021b; Skibba et al., 1970). In both A375 and MNT-1 human melanoma cells, neither HM nor DTIC increased caspase 3/7 activity following a 24 h incubation period. For DTIC, similar results have been described by other researchers. For instance, Bedia and colleagues (Bedia et al., 2011) incubated A375 cells with DTIC at 549 μM and reported that the activation of caspase 3 was only achieved after 48 h, indicating that apoptosis was not an early event (Bedia et al., 2011). On the other hand, Da-Costa-Rocha and coworkers (Da-Costa-Rocha and Prieto, 2021) did not observe caspase 3/7

activation 24 h after B16-F10 incubation with either DTIC or TMZ, at concentrations ranging from 1 to 2 mM (Da-Costa-Rocha and Prieto, 2021). Similarly, in our previous results using this murine cell line, although 24 h after incubation with HM and TMZ caspase 3/7 activity was close to controls, at an earlier incubation time (4 h) a significant increase was attained (Pinho et al., 2023). This may be due to the fact that activation of the caspase cascade does not always lead to apoptosis. In fact, the increase on caspase-3/7 activity induced by HM at 4 h may be related with cell cycle regulation, as reviewed by Lamkanfi and co-workers (Lamkanfi et al., 2007). Indeed, in our previous work we observed that B16-F10 exposure to HM resulted in a huge reduction of cell concentration (around 4-fold) in comparison to control (Pinho et al., 2023).

Regarding the cell cycle distribution, the observed effects in the present work were cell line dependent. HM and DTIC led to a cell cycle arrest at G0/G1 phase in A375 cells, while in MNT-1 an increase on S phase was observed only for HM. In previous research, incubation of B16-F10 cells with HM at 50 μM also resulted in a cell cycle arrest at G0/G1 phase, but at a much higher extent (2.3 fold *vs* control) (Pinho et al., 2023). These data may be explained by the pharmacological activity of triazenes that is related to DNA methylation promoted by methyldiazonium ion (Granada et al., 2021; Marchesi et al., 2007). This damage in the genetic material leads to a halt in cell cycle progression and subsequent apoptotic cell death (Marchesi et al., 2007; Noonan et al., 2012). Although it is described that DTIC can interfere in all cell cycle phases (Marchesi et al., 2007), such effect was not observed in the present work for MNT-1 cells. For instance, researchers have reported a S phase halt in A375 cells after incubation with DTIC (1000 or 2000 μM) (Koprowska et al., 2013). On the other hand, the exposure of A375 cells to DTIC at 40 μM resulted in a significant decrease of the percentage of cells in G0/G1 phase (Al-Qatati and Aliwaini, 2017). In the present work, on the opposite, DTIC at 70 μM induced a significant increase in G0/G1 phase.

As aforementioned, it is necessary to assess the antitumor activity in different melanoma cell models, since the obtained responses may vary depending on the cell line and compound under study as evidenced by several reports in the literature. For instance, researchers tested an estrogen receptor β agonist and distinct cell cycle results were achieved for two melanoma cell lines. In A375, an arrest at phase G0/G1 was observed, while in SK-Mel 30 cells the compound induced a G2/M arrest (Pontecorvi et al., 2022). In other studies, A375, MNT-1 and B16-F10 cells were exposed to doxorubicin. Results showed a cell cycle halt at the G0/G1 phase in A375 cells; however, in MNT-1 cells the drug did not induce any changes, even at high concentrations (Salvador et al., 2022). On the other hand, in B16-F10, doxorubicin induced an arrest at the G2/M phase (Mukherjee et al., 2020). Moreover, it has also been reported the cell cycle effects of an Akt inhibitor together with palmitic acid in A375 and B16-F10 cells. Once more, results were cell line-dependent: an arrest at G0/G1 phase in A375 cells while no effect in the murine melanoma cells (Kwan et al., 2014).

The developed HM liposomes (LIP HM; Table S1) presented similar physicochemical properties as the ones from the previous study (Pinho et al., 2023), exhibiting high incorporation parameters, low mean size, high homogeneity and a zeta potential close to neutrality. The high reproducibility is based on the method for liposomes preparation (Gaspar et al., 2015; Nave et al., 2016).

The *in vitro* antitumor activity of HM in free and liposomal forms was assessed using A375, MNT-1 and melanoma cells derived from biopsy samples of patients provided by IPO (IPO) (Table S2). Prior experiments with HM in the free form revealed IC_{50} values of 38.7 μM and > 75 μM for A375 and MNT-1 cells, respectively (Pinho et al., 2023). For the clinically derived cells, IPO, HM in the free form exhibited an IC_{50} value of 25 μM, demonstrating higher antiproliferative properties compared to DTIC (IC_{50} value > 75 μM). However, for all human cell lines, LIP HM displayed IC_{50} values > 75 μM. Comparable results were also observed in the murine melanoma cell line B16-F10 (Pinho et al., 2023). In this earlier work, despite LIP HM being successfully internalized by B16-F10 cells, similar low antiproliferative effect was also observed. This was attributed to the stable accommodation of the hydrophobic compound in the lipid bilayer of liposomes, as demonstrated by the high stability of LIP HM in the presence of human plasma, in suspension and in the lyophilized form. Moreover, nuclear magnetic resonance studies further confirmed the strong insertion of HM within the lipid bilayer (Pinho et al., 2023).

As aforementioned, *in vitro* assays with human melanoma cells provided valuable information regarding cytotoxicity and mode of action of drug candidates. Nevertheless, they can only estimate to a certain extent the anticancer efficacy and safety of tested compounds (Matias et al., 2021). Accordingly, it is required further validation using appropriate experimental animal models. The lack of a single murine model able to completely replicate the complexity of human melanoma, entails the use of different *in vivo* models (Matias et al., 2021). Of particular relevance are xenograft murine models that are established using either human cancer cell lines or patient-derived cells (Matias et al., 2021; Rebecca et al., 2020). For these studies, nude (nu/nu) mice, characterized by the absence of a thymus and T-cell deficiency, were the first and are still the most commonly used model in cancer research (Hirenallur-Shanthappa et al., 2017; Matias et al., 2021). In our previous research, the preclinical evaluation of HM formulations, in both subcutaneous and metastatic melanoma models using immunocompetent animals, demonstrated the significant high antitumor effect of LIP HM (Pinho et al., 2023).

Based on these promising results, in the current work the antimelanoma activity of LIP HM was further validated in immunocompromised animals. Melanoma induction protocol was firstly optimized by evaluating groups of athymic nude mice after i.v. injection of A375 or MNT-1 cells. Histopathological analysis revealed that multiple cell clusters were found on the pleural surface of mice induced with A375. In turn, no alterations were detected in case of animals that received MNT-1 cells (data not shown). In addition, HM exhibited higher antiproliferative properties towards A375 *vs* MNT-1 and displayed a similar cell cycle effect than DTIC, the positive control (Fig. 2). Furthermore, A375 is one of the most commonly used human melanoma cell line for compound screening and mouse xenograft development (Couto et al., 2019). For these reasons, the *in vivo* experiments for therapeutic evaluation of HM formulations were conducted using the A375 cell line. The establishment of this experimental model was accomplished by s.c. injection of these human cells into immunodeficient nude mice (Matias et al., 2021), thus generating a tumor comparable to melanoma metastasis in the skin (Beaumont et al., 2014). This model allows the interaction of malignant cells with the stroma and surrounding lymphatic and blood vessels, simulating the melanoma dynamics that occurs in patients (Avram et al., 2017; Rebecca et al., 2020).

In A375 melanoma model, treatment with LIP HM significantly impaired tumor progression, displaying the lowest tumor volume and tumor weight when compared to the other tested groups. Specifically, LIP HM led to a 4-, 5-, and 6-fold lower tumor volumes compared to DTIC, Free HM and Control, respectively. The significantly reduced tumor growth here observed is indicative of LIP HM effectiveness against melanoma metastasis, as previously confirmed in a B16-F10 murine model (Pinho et al., 2023).

The remarkable antimelanoma effect of LIP HM is correlated with the passive accumulation of liposomes at tumor sites (Allen and Cullis, 2004; Crommelin et al., 2020; Dos Santos et al., 2007; Maeda et al., 2000; Pinho et al., 2023). Of note, LIP HM displays long blood circulating properties due to the presence of DSPE-PEG at liposomal surface. The *in vivo* biodistribution profile of LIP HM has been recently assessed. Indeed, 48 h after administration of LIP HM, up to 4% of the injected dose was detected in melanoma mass tumors (Pinho et al., 2023). This was a notable achievement, since preclinical studies using other nanoparticulate systems accomplish < 1% of injected dose at tumor sites (Belfiore et al., 2018; De Silva et al., 2022; Sindhwani et al., 2020; Wilhelm et al., 2016).

To investigate the mechanism underlying the antitumor effect of LIP HM, caspase 3/7 activity, a marker of apoptosis, was assessed in total protein extracts from mass tumors. Although, *in vitro*, HM did not induce changes in caspase 3/7 activity, 24 h after incubation, a significant increase for animals treated with LIP HM compared to control group was achieved. Tumor microenvironment, comprising fibroblasts, endothelial cells, adipocytes and other cell types may influence the response of cancer cells to compounds (Matias et al., 2021). Although for animals that received i.v. administrations of DTIC and HM in the free form an increase on caspase 3/7 activity was attained, these differences were not statistically significant compared to control group. These results clearly demonstrate the therapeutic advantages of associating potent antiproliferative compounds to drug delivery systems, such as liposomes.

The safety of tested formulations was evaluated through tissue indexes and hepatic biomarkers. Alterations in organ weight are recognized as a sensitive indicator of potential toxic effects in organ integrity, being assessed through organ-to-body weight ratios (tissue index). Elevated values indicate organ hypertrophy, edema or congestion and, in turn, a decreased tissue index indicates organ atrophy and degeneration (Michael et al., 2007; Pinho et al., 2021a; Sellers et al., 2007; Xu et al., 2013). Here, no major differences between groups were observed in terms of tissue index, denoting the safety of tested formulations. Moreover, liver transaminases AST and ALT are highly present in hepatocytes and elevated serum levels of these enzymes indicate acute or chronic liver damage (Kew, 2000; Yang et al., 2017). In this work, the obtained values were within reference intervals and have been previously reported by other authors (Charles River Laboratories, 2012; Miguel et al., 2022; Yang et al., 2020). The lower serum levels of AST observed for mice treated with LIP HM suggests a protective effect. Similar reports have also been described in literature, namely a hybrid molecule composed of a nucleoside group and betulinic acid (Zheng et al., 2022) and an amine-linked NO-donor-tacrine hybrid (Fang et al., 2008). In addition, the AST/ALT ratio is frequently used as a key indicator of hepatic injury, with a high value being associated with a severe condition (Wang et al., 2016). Here, animals treated with LIP HM displayed a ratio < 1, thus demonstrating its safety.

5. Conclusions

The inherent complexity of melanoma is difficult to mimic in preclinical assays thus requiring the use of different *in vitro* and *in vivo* models aiming to provide a more reliable prediction of clinical responses of new therapies.

Overall, the proof-of-concept in the human melanoma model herein described contributes for the validation of LIP HM potential as an effective and safe therapeutic strategy against melanoma. This nanomedicine constitutes an important step forward that may advance towards clinical translation.

Institutional review board statement

The study was conducted in accordance with the Declaration of Helsinki and approved by the Ethics Committee of the Faculty of Pharmacy, Universidade de Lisboa (PTDC/MED-QUI/31721/2017, 10/02/2020). The animal study protocol was approved by the Animal Welfare Body (ORBEA) of the Faculty of Pharmacy, Universidade de Lisboa (PTDC/MED-QUI/31721/2017, 02/01/2018), permitted by the competent national authority *Direção-Geral de Alimentação e Veterinária* (DGAV) and in accordance with the EU Directive (2010/63/UE) and Portuguese laws (DR 113/2013, 2880/ 2015, 260/2016 and 1/2019) for the use and care of animals in research.

Informed consent statement

Informed consent was obtained from all subjects involved in the study.

Data availability statement

Data is available upon request.

CRediT authorship contribution statement

Jacinta O. Pinho: Formal analysis, Investigation, Writing – original draft. **Mariana Matias:** Formal analysis, Investigation, Writing – original draft. **Ana Godinho-Santos:** Investigation. **Joana D. Amaral:** Investigation. **Eduarda Mendes:** Methodology. **Maria Jesus Perry:** Methodology. **Ana Paula Francisco:** Methodology, Writing – review & editing. **Cecília M.P. Rodrigues:** Conceptualization, Resources, Writing – review & editing, Supervision, Project administration, Funding acquisition. **M. Manuela Gaspar:** Conceptualization, Resources, Writing – review & editing, Supervision, Project administration, Funding acquisition.

Declaration of Competing Interest

The authors declare that they have no known competing financial interests or personal relationships that could have appeared to influence the work reported in this paper.

Data availability

Data will be made available on request.

Acknowledgments

This research was funded by Fundação para a Ciência e Tecnologia (FCT), through projects UIDB/04138/2020, UIDP/ 04138/2020, PTDC/MED-QUI/31721/2017 and by a PhD grant SFRH/BD/117586/2016. The authors also acknowledge the Phospholipid Research Center (PRC) for the financial support Grant number: MMG-2021-092/1-1 and Secção Regional do Sul e Regiões Autónomas da Ordem dos Farmacêuticos (SRSRA-OF) through an innovation grant (BInov). The authors would like to express their thanks to Dr. Joaninha Costa Rosa, from the Histopathology Laboratory of IPO Lisboa, for helping in the process of obtaining cells from melanoma patients.

Appendix A. Supplementary data

Supplementary data to this article can be found online at https://doi.org/10.1016/j.ijpharm.2023.123011.

References

Allen, T.M., Cullis, P.R., 2004. Drug delivery systems: Entering the mainstream. Science 303, 1818–1822. https://doi.org/10.1126/science.1095833.

Al-Qatati, A., Aliwaini, S., 2017. Combined pitavastatin and dacarbazine treatment activates apoptosis and autophagy resulting in synergistic cytotoxicity in melanoma cells. Oncol. Lett. 14, 7993–7999. https://doi.org/10.3892/ol.2017.7189.

Alsayari, A., Asiri, Y.I., Muhsinah, A.B., Hassan, M.Z., 2022. Synthesis of new pyrazole hybrids as potential anticancer agents with xanthine oxidase inhibitory activity. Anticancer. Agents Med. Chem. 22, 2303–2309. https://doi.org/10.2174/1871520622666220110162651.

Aly, A.A., Bräse, S., Hassan, A.A., Mohamed, N.K., El-Haleem, L.E.A., Nieger, M., Morsy, N.M., Alshammari, M.B., Ibrahim, M.A.A., Abdelhafez, E.M.N., 2020. Design, synthesis, and molecular docking of paracyclophanyl-thiazole hybrids as novel CDK1 inhibitors and apoptosis inducing anti-melanoma agents. Molecules 25, 5569. https://doi.org/10.3390/molecules25235569.

Avram, S., Coricovac, D.-E., Pavel, I.Z., Pinzaru, I., Ghiulai, R., Baderca, F., Soica, C., Muntean, D., Branisteanu, D.E., Spandidos, D.A., Tsatsakis, A.M., Dehelean, C.A., 2017. Standardization of A375 human melanoma models on chicken embryo chorioallantoic membrane and Balb/c nude mice. Oncol. Rep. 38, 89–99. https://doi.org/10.3892/or.2017.5658.

Barrionuevo, E., Cayrol, F., Cremaschi, G.A., Cornier, P.G., Boggián, D.B., Delpiccolo, C. M.L., Mata, E.G., Roguin, L.P., Blank, V.C., 2020. A penicillin derivative exerts an anti-metastatic activity in melanoma cells through the downregulation of integrin αvβ3 and Wnt/β-catenin pathway. Front. Pharmacol. 11, 127 https://doi.org/10.3389/fphar.2020.00127.

Beaumont, K., Mohana-Kumaran, N., Haass, N., 2014. Modeling melanoma in vitro and in vivo. Healthcare 2, 27–46. https://doi.org/10.3390/healthcare2010027.
Bedia, C., Casas, J., Andrieu-Abadie, N., Fabriàs, G., Levade, T., 2011. Acid ceramidase expression modulates the sensitivity of A375 melanoma cells to dacarbazine. J. Biol. Chem. 286, 28200–28209. https://doi.org/10.1074/jbc.M110.216382.
Belfiore, L., Saunders, D.N., Ranson, M., Thurecht, K.J., Storm, G., Vine, K.L., 2018. Towards clinical translation of ligand-functionalized liposomes in targeted cancer therapy: Challenges and opportunities. J. Control. Release 277, 1–13. https://doi.org/10.1016/j.jconrel.2018.02.040.
Bratu, L.M., Marcovici, I., Macasoi, I., Manea, A., Niculescu, B., Olaru, F., Heghes, A., Dehelean, C., Coricovac, D., 2022. In vitro insights regarding the role of melanin in melanoma cells' response to betulinic acid treatment. Farmacia 70, 8–16. https://doi.org/10.31925/farmacia.2022.1.2.
Brożyna, A.A., Jóźwicki, W., Carlson, J.A., Slominski, A.T., 2013. Melanogenesis affects overall and disease-free survival in patients with stage III and IV melanoma. Hum. Pathol. 44, 2071–2074. https://doi.org/10.1016/j.humpath.2013.02.022.
Charles River Laboratories, 2012. C57BL/6 Mice [WWW Document]. URL https://www.criver.com/sites/default/files/resources/C57BL6MouseClinicalPathologyData.pdf (accessed 11.5.22).
Couto, G.K., Segatto, N.V., Oliveira, T.L., Seixas, F.K., Schachtschneider, K.M., Collares, T., 2019. The melding of drug screening platforms for melanoma. Front. Oncol. 9, 512 https://doi.org/10.3389/fonc.2019.00512.
Crommelin, D.J.A., van Hoogevest, P., Storm, G., 2020. The role of liposomes in clinical nanomedicine development. What now? Now what? J. Control. Release 318, 256–263. https://doi.org/10.1016/j.jconrel.2019.12.023.
Da-Costa-Rocha, I., Prieto, J.M., 2021. In vitro effects of selective COX and LOX inhibitors and their combinations with antineoplastic drugs in the mouse melanoma cell line B16F10. Int. J. Mol. Sci. 22, 6498 https://doi.org/10.3390/ijms22126498.
De Silva, L., Fu, J.-Y., Htar, T.T., Wan Kamal, W.H.B., Kasbollah, A., Muniyandy, S., Chuah, L.-H., 2022. Biodistribution study of niosomes in tumor-implanted BALB/C mice using scintigraphic imaging. Front. Pharmacol. 12 https://doi.org/10.3389/fphar.2021.778396.
Dos Santos, N., Allen, C., Doppen, A.-M., Anantha, M., Cox, K.A.K., Gallagher, R.C., Karlsson, G., Edwards, K., Kenner, G., Samuels, L., Webb, M.S., Bally, M.B., 2007. Influence of poly(ethylene glycol) grafting density and polymer length on liposomes: Relating plasma circulation lifetimes to protein binding. Biochim. Biophys. Acta - Biomembr. 1768, 1367–1377. https://doi.org/10.1016/j.bbamem.2006.12.013.
Dzwierzynski, W.W., 2021. Melanoma risk factors and prevention. Clin. Plast. Surg. 48, 543–550. https://doi.org/10.1016/j.cps.2021.05.001.
Fang, L., Appenroth, D., Decker, M., Kiehntopf, M., Roegler, C., Deufel, T., Fleck, C., Peng, S., Zhang, Y., Lehmann, J., 2008. Synthesis and biological evaluation of NO-donor-tacrine hybrids as hepatoprotective anti-Alzheimer drug candidates. J. Med. Chem. 51, 713–716. https://doi.org/10.1021/jm701491k.
Francisco, A.P., Mendes, E., Santos, A.R., Perry, M.J., 2019. Anticancer triazenes: From bioprecursors to hybrid molecules. Curr. Pharm. Des. 25, 1623–1642. https://doi.org/10.2174/1381612825666190617155749.
Gaspar, M.M., Calado, S., Pereira, J., Ferronha, H., Correia, I., Castro, H., Tomás, A.M., Cruz, M.E.M., 2015. Targeted delivery of paromomycin in murine infectious diseases through association to nano lipid systems. Nanomedicine Nanotechnology. Biol. Med. 11, 1851–1860. https://doi.org/10.1016/j.nano.2015.06.008.
GLOBOCAN., 2022. Estimated number of new cases from 2020 to 2040, Both sexes, age [0-85+] - Melanoma of skin [WWW Document]. URL https://gco.iarc.fr/tomorrow/en/dataviz/isotype?types=0&sexes=0&mode=population&group_populations=1&multiple_populations=1&multiple_cancers=0&cancers=16&populations=903_904_905_908_909_935&single_unit=10000 (accessed 1.25.22).
Granada, M., Mendes, E., Perry, M.J., Penetra, M.J., Gaspar, M.M., Pinho, J.O., Serra, S., António, C.T., Francisco, A.P., 2021. Sulfur analogues of tyrosine in the development of triazene hybrid compounds: A new strategy against melanoma. ACS Med. Chem. Lett. 12, 1669–1677. https://doi.org/10.1021/acsmedchemlett.1c00252.
Hirenallur-Shanthappa, D.K., Ramírez, J.A., Iritani, B.M., 2017. Chapter 5 - Immunodeficient Mice: The Backbone of Patient-Derived Tumor Xenograft Models, in: Uthamanthil, R., Tinkey (Eds.), Patient Derived Tumor Xenograft Models. Elsevier, pp. 57–73. https://doi.org/10.1016/B978-0-12-804010-2.00005-9.
Hoek, K., Rimm, D.L., Williams, K.R., Zhao, H., Ariyan, S., Lin, A., Kluger, H.M., Berger, A.J., Cheng, E., Trombetta, E.S., Wu, T., Niinobe, M., Yoshikawa, K., Hannigan, G.E., Halaban, R., 2004. Expression profiling reveals novel pathways in the transformation of melanocytes to melanomas. Cancer Res. 64, 5270–5282. https://doi.org/10.1158/0008-5472.CAN-04-0731.
Ito, T., Tanaka, Y., Murata, M., Kaku-Ito, Y., Furue, K., Furue, M., 2021. BRAF heterogeneity in melanoma. Curr. Treat. Options Oncol. 22, 20 https://doi.org/10.1007/s11864-021-00818-3.
Jia, D., Yang, Y., Yuan, F., Fan, Q., Wang, F., Huang, Y., Song, H., Hu, P., Wang, R., Li, G., Liu, R., Li, J., 2020. Increasing the antitumor efficacy of doxorubicin liposomes with coupling an anti-EGFR affibody in EGFR-expressing tumor models. Int. J. Pharm. 586, 119541 https://doi.org/10.1016/j.ijpharm.2020.119541.
Jimbow, K., Ishii-Osai, Y., Ito, S., Tamura, Y., Ito, A., Yoneta, A., Kamiya, T., Yamashita, T., Honda, H., Wakamatsu, K., Murase, K., Nohara, S., Nakayama, E., Hasegawa, T., Yamamoto, I., Kobayashi, T., 2013. Melanoma-targeted chemothermotherapy and in situ peptide immunotherapy through HSP production by using melanogenesis substrate, NPrCAP, and magnetite nanoparticles. J. Skin Cancer 2013, 742925. https://doi.org/10.1155/2013/742925.
Kew, M.C., 2000. Serum aminotransferase concentration as evidence of hepatocellular damage. Lancet (London, England) 355, 591–592. https://doi.org/10.1016/S0140-6736(99)00219-6.
Koprowska, K., Hartman, M.L., Sztiller-Sikorska, M., Czyz, M.E., 2013. Parthenolide enhances dacarbazine activity against melanoma cells. Anticancer. Drugs 24, 835–845. https://doi.org/10.1097/CAD.0b013e3283635a04.
Kwan, H.Y., Fu, X., Liu, B., Chao, X., Chan, C.L., Cao, H., Su, T., Tse, A.K.W., Fong, W.F., Yu, Z.-L., 2014. Subcutaneous adipocytes promote melanoma cell growth by activating the Akt signaling pathway. J. Biol. Chem. 289, 30525–30537. https://doi.org/10.1074/jbc.M114.593210.
Lamkanfi, M., Festjens, N., Declercq, W., Berghe, T.V., Vandenabeele, P., 2007. Caspases in cell survival, proliferation and differentiation. Cell Death Differ 14, 44–55. https://doi.org/10.1038/sj.cdd.4402047.
Lasch, J., Weissig, V., Brandl, M., 2003. Preparation of Liposomes. In: Torchilin, V., Weissig, V. (Eds.), Liposomes: A Practical Approach. Oxford University Press, Oxford, UK, pp. 3–27. https://books.google.co.in/books?hl=en&lr=&id=ClEJl4FIzrIC&oi=fnd&pg=PR13&dq=Liposomes:+A+Practical+Approach.+Oxford+University+Press,+Oxford,+UK,+pp.+3%E2%80%9327&ots=43kGWz3-o2&sig=bKrrwhxVCwcZh9eLJhUaQfqsxK4.
Li, C., Wang, Q., Shen, S., Wei, X., Li, G., 2019. HIF-1α/VEGF signaling-mediated epithelial-mesenchymal transition and angiogenesis is critically involved in anti-metastasis effect of luteolin in melanoma cells. Phyther. Res. 33, 798–807. https://doi.org/10.1002/ptr.6273.
Liu, W., Dowling, J.P., Murray, W.K., McArthur, G.A., Thompson, J.F., Wolfe, R., Kelly, J. W., 2006. Rate of growth in melanomas. Arch. Dermatol. 142, 1551–1558. https://doi.org/10.1001/archderm.142.12.1551.
Maeda, H., Wu, J., Sawa, T., Matsumura, Y., Hori, K., 2000. Tumor vascular permeability and the EPR effect in macromolecular therapeutics: A review. J. Control. Release 65, 271–284. https://doi.org/10.1016/S0168-3659(99)00248-5.
Makowiecka, A., Simiczyjew, A., Nowak, D., Mazur, A.J., 2016. Varying effects of EGF, HGF and TGFβ on formation of invadopodia and invasiveness of melanoma cell lines of different origin. Eur. J. Histochem. 60, 2728. https://doi.org/10.4081/ejh.2016.2728.
Marchesi, F., Turriziani, M., Tortorelli, G., Avvisati, G., Torino, F., Devecchis, L., 2007. Triazene compounds: Mechanism of action and related DNA repair systems. Pharmacol. Res. 56, 275–287. https://doi.org/10.1016/j.phrs.2007.08.003.
Massand, S., Neves, R.I., 2021. Emerging therapies in the treatment of advanced melanoma. Clin. Plast. Surg. 48, 713–733. https://doi.org/10.1016/j.cps.2021.06.008.
Matias, M., Pinho, J.O., Penetra, M.J., Campos, G., Reis, C.P., Gaspar, M.M., 2021. The challenging melanoma landscape: From early drug discovery to clinical approval. Cells 10, 3088. https://doi.org/10.3390/cells10113088.
Matos, C.P., Albino, M., Lopes, J., Viana, A.S., Côrte-Real, L., Mendes, F., Pessoa, J.C., Tomaz, A.I., Reis, C.P., Gaspar, M.M., Correia, I., 2022. New iron(III) anti-cancer aminobisphenolate/phenanthroline complexes: Enhancing their therapeutic potential using nanoliposomes. Int. J. Pharm. 623, 121925 https://doi.org/10.1016/j.ijpharm.2022.121925.
Melnikova, V.O., Bolshakov, S.V., Walker, C., Ananthaswamy, H.N., 2004. Genomic alterations in spontaneous and carcinogen-induced murine melanoma cell lines. Oncogene 23, 2347–2356. https://doi.org/10.1038/sj.onc.1207405.
Michael, B., Yano, B., Sellers, R.S., Perry, R., Morton, D., Roome, N., Johnson, J.K., Schafer, K., 2007. Evaluation of organ weights for rodent and non-rodent toxicity Studies: A review of regulatory guidelines and a survey of current practices. Toxicol. Pathol. 35, 742–750. https://doi.org/10.1080/01926230701595292.
Miguel, F.M., Picada, J.N., da Silva, J.B., Schemitt, E.G., Colares, J.R., Hartmann, R.M., Marroni, C.A., Marroni, N.P., 2022. Melatonin attenuates inflammation, oxidative stress, and DNA damage in mice with nonalcoholic steatohepatitis induced by a methionine- and choline-deficient diet. Inflammation 45, 1968–1984. https://doi.org/10.1007/s10753-022-01667-4.
Militaru, I.V., Rus, A.A., Munteanu, C.V.A., Manica, G., Petrescu, S.M., 2023. New panel of biomarkers to discriminate between amelanotic and melanotic metastatic melanoma. Front. Oncol. 12 https://doi.org/10.3389/fonc.2022.1061832.
Mukherjee, S., Kotcherlakota, R., Haque, S., Bhattacharya, D., Kumar, J.M., Chakravarty, S., Patra, C.R., 2020. Improved delivery of doxorubicin using rationally designed PEGylated platinum nanoparticles for the treatment of melanoma. Mater. Sci. Eng. C 108, 110375. https://doi.org/10.1016/j.msec.2019.110375.
Nave, M., Castro, R.E., Rodrigues, C.M., Casini, A., Soveral, G., Gaspar, M.M., 2016. Nanoformulations of a potent copper-based aquaporin inhibitor with cytotoxic effect against cancer cells. Nanomedicine (Lond) 11, 1817–1830. https://doi.org/10.2217/nnm-2016-0086.
Noonan, E.M., Shah, D., Yaffe, M.B., Lauffenburger, D.A., Samson, L.D., 2012. O 6-Methylguanine DNA lesions induce an intra-S-phase arrest from which cells exit into apoptosis governed by early and late multi-pathway signaling network activation. Integr. Biol. 4, 1237–1255. https://doi.org/10.1039/c2ib20091k.
Pereira, D.M., Simões, A.E.S., Gomes, S.E., Castro, R.E., Carvalho, T., Rodrigues, C.M.P., Borralho, P.M., 2016. MEK5/ERK5 signaling inhibition increases colon cancer cell sensitivity to 5-fluorouracil through a p53-dependent mechanism. Oncotarget 7, 34322–34340. https://doi.org/10.18632/oncotarget.9107.
Pinho, J.O., Amaral, J.D., Castro, R.E., Rodrigues, C.M.P., Casini, A., Soveral, G., Gaspar, M.M., 2019a. Copper complex nanoformulations featuring highly promising therapeutic potential in murine melanoma models. Nanomedicine 14, 835–850. https://doi.org/10.2217/nnm-2018-0388.
Pinho, J.O., da Silva, I.V., Amaral, J.D., Rodrigues, C.M.P., Casini, A., Soveral, G., Gaspar, M.M., 2021a. Therapeutic potential of a copper complex loaded in pH-sensitive long circulating liposomes for colon cancer management. Int. J. Pharm. 599, 120463 https://doi.org/10.1016/j.ijpharm.2021.120463.
Pinho, J.O., Lopes, J., Albino, M., Reis, C., Matias, M., Gaspar, M.M., 2021b. Advances in nanotechnology-related strategies against melanoma, in: de Oliveira, M.R. (Ed.),

Mitochondrial Dysfunction and Nanotherapeutics. Elsevier, pp. 385–424. https://doi.org/10.1016/B978-0-323-85666-9.00009-7.

Pinho, J.O., Matias, M., Gaspar, M.M., 2019b. Emergent nanotechnological strategies for systemic chemotherapy against melanoma. Nanomaterials 9, 1455. https://doi.org/10.3390/nano9101455.

Pinho, J.O., Matias, M., Marques, V., Eleutério, C., Fernandes, C., Gano, L., Amaral, J.D., Mendes, E., Perry, M.J., Moreira, J.N., Storm, G., Francisco, A.P., Rodrigues, C.M.P., Gaspar, M.M., 2023. Preclinical validation of a new hybrid molecule loaded in liposomes for melanoma management. Biomed. Pharmacother. 157, 114021 https://doi.org/10.1016/j.biopha.2022.114021.

Pontecorvi, G., Bellenghi, M., Tait, S., Tirelli, V., Matarrese, P., Mattia, G., Carè, A., Puglisi, R., 2022. Different susceptibilities of human melanoma cell lines to G2/M blockage and cell death activation in response to the estrogen receptor β agonist LY500307. J. Cancer 13, 1573–1587. https://doi.org/10.7150/jca.65425.

Rebecca, V.W., Somasundaram, R., Herlyn, M., 2020. Pre-clinical modeling of cutaneous melanoma. Nat. Commun. 11, 2858 https://doi.org/10.1038/s41467-020-15546-9.

Rok, J., Rzepka, Z., Kowalska, J., Banach, K., Beberok, A., Wrześniok, D., 2022. The anticancer potential of doxycycline and minocycline—A comparative study on amelanotic melanoma cell lines. Int. J. Mol. Sci. 23, 831 https://doi.org/10.3390/ijms23020831.

Rossi, S., Cordella, M., Tabolacci, C., Nassa, G., D'Arcangelo, D., Senatore, C., Pagnotto, P., Magliozzi, R., Salvati, A., Weisz, A., Facchiano, A., Facchiano, F., 2018. TNF-alpha and metalloproteases as key players in melanoma cells aggressiveness. J. Exp. Clin. Cancer Res. 37, 326 https://doi.org/10.1186/s13046-018-0982-1.

Rouser, G., Fleischer, S., Yamamoto, A., 1970. Two dimensional thin layer chromatographic separation of polar lipids and determination of phospholipids by phosphorus analysis of spots. Lipids 5, 494–496. https://doi.org/10.1007/BF02531316.

Ryabaya, O.O., Abramov, I.S., Khochenkov, D.A., Akasov, R., Sholina, N.V., Prokofieva, A.A., 2021. Rapamycin synergizes the cytotoxic effects of MEK inhibitor binimetinib and overcomes acquired resistance to therapy in melanoma cell lines in vitro. Invest. New Drugs 39, 987–1000. https://doi.org/10.1007/s10637-021-01089-3.

Ryabaya, O., Prokofieva, A., Akasov, R., Khochenkov, D., Emelyanova, M., Burov, S., Markvicheva, E., Inshakov, A., Stepanova, E., 2019. Metformin increases antitumor activity of MEK inhibitor binimetinib in 2D and 3D models of human metastatic melanoma cells. Biomed. Pharmacother. 109, 2548–2560. https://doi.org/10.1016/j.biopha.2018.11.109.

Salvador, D., Bastos, V., Oliveira, H., 2022. Hyperthermia enhances doxorubicin therapeutic efficacy against A375 and MNT-1 melanoma cells. Int. J. Mol. Sci. 23, 35 https://doi.org/10.3390/ijms23010035.

Santos-Rebelo, A., Garcia, C., Eleutério, C., Bastos, A., Coelho, S.C., Coelho, M.A.N., Molpeceres, J., Viana, A.S., Ascensão, L., Pinto, J.F., Gaspar, M.M., Rijo, P., Reis, C. P., 2018. Development of parvifloron D-loaded smart nanoparticles to target pancreatic cancer. Pharmaceutics 10, 216. https://doi.org/10.3390/pharmaceutics10040216.

Sellers, R.S., Mortan, D., Michael, B., Roome, N., Johnson, J.K., Yano, B.L., Perry, R., Schafer, K., 2007. Society of toxicologic pathology position paper: Organ weight recommendations for toxicology studies. Toxicol. Pathol. 35, 751–755. https://doi.org/10.1080/01926230701595300.

Sindhwani, S., Syed, A.M., Ngai, J., Kingston, B.R., Maiorino, L., Rothschild, J., MacMillan, P., Zhang, Y., Rajesh, N.U., Hoang, T., Wu, J.L.Y., Wilhelm, S., Zilman, A., Gadde, S., Sulaiman, A., Ouyang, B., Lin, Z., Wang, L., Egeblad, M., Chan, W.C.W., 2020. The entry of nanoparticles into solid tumours. Nat. Mater. 19, 566–575. https://doi.org/10.1038/s41563-019-0566-2.

Skibba, J.L., Beal, D.D., Ramirez, G., Bryan, G.T., 1970. N-demethylation of the antineoplastic agent 4(5)-(3,3-dimethyl-1-triazeno)imidazole-5(4)-carboxamide by rats and man. Cancer Res. 30, 147–150. https://aacrjournals.org/cancerres/article/30/1/147/477698/N-Demethylation-of-the-Antineoplastic-Agent-4-5-3.

Slominski, R.M., Sarna, T., Płonka, P.M., Raman, C., Brożyna, A.A., Slominski, A.T., 2022. Melanoma, melanin, and melanogenesis: The Yin and Yang relationship. Front. Oncol. 12 https://doi.org/10.3389/fonc.2022.842496.

Slominski, A., Tobin, D.J., Shibahara, S., Wortsman, J., 2004. Melanin pigmentation in mammalian skin and its hormonal regulation. Physiol. Rev. 84, 1155–1228. https://doi.org/10.1152/physrev.00044.2003.

Sun, M., Qin, J., Kang, Y., Zhang, Y., Ba, M., Yang, H., Duan, Y., Yao, Y., 2022. 2-Methoxydiol derivatives as new tubulin and HDAC dual-targeting inhibitors, displaying antitumor and antiangiogenic response. Bioorg. Chem. 120, 105625 https://doi.org/10.1016/j.bioorg.2022.105625.

Sun, C., Wang, L., Huang, S., Heynen, G.J.J.E., Prahallad, A., Robert, C., Haanen, J., Blank, C., Wesseling, J., Willems, S.M., Zecchin, D., Hobor, S., Bajpe, P.K., Lieftink, C., Mateus, C., Vagner, S., Grernrum, W., Hofland, I., Schlicker, A., Wessels, L.F.A., Beijersbergen, R.L., Bardelli, A., Di Nicolantonio, F., Eggermont, A. M.M., Bernards, R., 2014. Reversible and adaptive resistance to BRAF(V600E) inhibition in melanoma. Nature 508, 118–122. https://doi.org/10.1038/nature13121.

Sweeny, L., Prince, A., Patel, N., Moore, L.S., Rosenthal, E.L., Hughley, B.B., Warram, J. M., 2016. Antiangiogenic antibody improves melanoma detection by fluorescently labeled therapeutic antibodies. Laryngoscope 126, E387–E395. https://doi.org/10.1002/lary.26215.

Szumilak, M., Wiktorowska-Owczarek, A., Stanczak, A., 2021. Hybrid drugs — A strategy for overcoming anticancer drug resistance? Molecules 26, 2601. https://doi.org/10.3390/molecules26092601.

Thomas, N.E., Kricker, A., Waxweiler, W.T., Dillon, P.M., Busam, K.J., From, L., Groben, P.A., Armstrong, B.K., Anton-Culver, H., Gruber, S.B., Marrett, L.D., Gallagher, R.P., Zanetti, R., Rosso, S., Dwyer, T., Venn, A., Kanetsky, P.A., Orlow, I., Paine, S., Ollila, D.W., Reiner, A.S., Luo, L., Hao, H., Frank, J.S., Begg, C.B., Berwick, M., 2014. Comparison of clinicopathologic features and survival of histopathologically amelanotic and pigmented melanomas. JAMA Dermatol. 150, 1306–1314. https://doi.org/10.1001/jamadermatol.2014.1348.

Viegas-Junior, C., Barreiro, E.J., Fraga, C.A.M., 2007. Molecular hybridization: A useful tool in the design of new drug prototypes. Curr. Med. Chem. 14, 1829–1852. https://doi.org/10.2174/092986707781058805.

Wang, R., Feng, X., Zhu, K., Zhao, X., Suo, H., 2016. Preventive activity of banana peel polyphenols on CCl4-induced experimental hepatic injury in Kunming mice. Exp. Ther. Med. 11, 1947–1954. https://doi.org/10.3892/etm.2016.3155.

Wilhelm, S., Tavares, A.J., Dai, Q., Ohta, S., Audet, J., Dvorak, H.F., Chan, W.C.W., 2016. Analysis of nanoparticle delivery to tumours. Nat. Rev. Mater. 1, 16014 https://doi.org/10.1038/natrevmats.2016.14.

Xu, J., Shi, H., Ruth, M., Yu, H., Lazar, L., Zou, B., Yang, C., Wu, A., Zhao, J., 2013. Acute toxicity of intravenously administered titanium dioxide nanoparticles in mice. PLoS One 8, e70618. https://doi.org/10.1371/journal.pone.0070618.

Yang, M., Sun, F., Zhou, Y., He, M., Yao, P., Peng, Y., Luo, F., Liu, F., 2020. Preventive effect of lemon seed flavonoids on carbon tetrachloride-induced liver injury in mice. RSC Adv 10, 12800–12809. https://doi.org/10.1039/D0RA01415J.

Yang, H., Wang, J., Fan, J., Zhang, Y., Zhao, J., Dai, X., Liu, Q., Shen, Y., Liu, C., Sun, W., Sun, Y., 2017. Ilexgenin A exerts anti-inflammation and anti-angiogenesis effects through inhibition of STAT3 and PI3K pathways and exhibits synergistic effects with Sorafenib on hepatoma growth. Toxicol. Appl. Pharmacol. 315, 90–101. https://doi.org/10.1016/j.taap.2016.12.008.

Zheng, L., Zou, X., Wang, Y., Zou, M., Ma, F., Wang, N., Li, J., Wang, M., Hung, H.-Y., Wang, Q., 2022. Betulinic acid-nucleoside hybrid prevents acute alcohol-induced liver damage by promoting anti-oxidative stress and autophagy. Eur. J. Pharmacol. 914, 174686 https://doi.org/10.1016/j.ejphar.2021.174686.